mper

Modeling of Wire EDM Using an Integrated Approach for Machining of AISI304 Stainless Steel

Sara A. EL-BAHLOUL[1,2]

[1] *Production and Mechanical Design Engineering Department, Faculty of Engineering, Mansoura University, Egypt*
[2] *Faculty of Engineering, New Mansoura University, Egypt*

Abstract
A non-traditional method of thermal machining called wire electrical discharge machining (WEDM) is utilized for the production of intricate and complex components, particularly those composed of difficult-to-machine materials. Stainless steel has gained widespread usage in various applications in contemporary industry owing to its exceptional properties. In this present investigation, a numerical 3D finite element modeling simulation was conducted using the ABAQUS software to analyze the Material Removal Rates (MRR) for both single and multi-discharge scenarios of AISI 304 stainless steel. The findings indicate a close correspondence between the MRR values predicted by the numerical modeling and those obtained experimentally corresponding to the optimal process parameters: $I = 6$ A, Ton = 45 µs, and Toff = 5 µs. Hence, this numerical approach offers the potential to forecast outcomes before actual machining operations.

Keywords
Wire Electrical Discharge Machining, Numerical modeling, AISI 304 stainless steel, Material Removal Rates, multi discharges.

Introduction

WEDM is an exceptional variant of Electrical Discharge Machining (EDM), distinguished by its utilization of a slender wire with reduced diameter as the electrode for the purpose of generating a minute kerf within the workpiece. This technique involves the removal of material through a number of brief discharges taking place amidst the workpiece and the wire, facilitated by the existence of dielectric fluid. The region experiencing the discharge encounters an elevated temperature, resulting in surface melting and subsequent removal. To ensure efficient evacuation of the eliminated particles, the dielectric medium is systematically circulated, thereby offering effective flushing capabilities (Kumar et al., 2018; Mythili and Thanigaivelan 2020). A schematic depiction of the WEDM process is presented in Fig. 1.
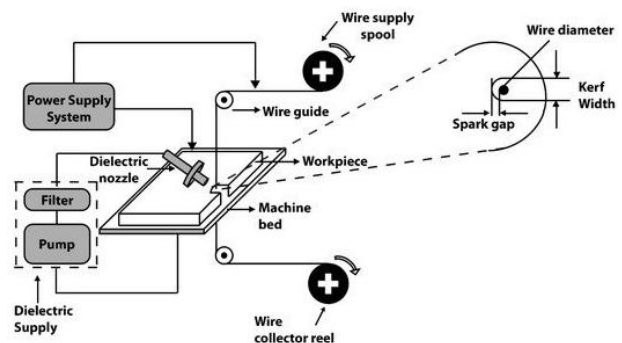
Fig. 1. Schematic diagram of WEDM

Due to the distinctive characteristics exhibited by stainless steel, such as its elevated coefficient of work-hardening, remarkable toughness, and commendable conductivity at minimal temperatures, in conjunction with its inherent qualities of being corrosion-resistant, oxidation-resistant, and possessing a lustrous surface, stainless steel materials have garnered extensive employment within numerous contemporary industrial sectors. However, notwithstanding these manifold advantages, stainless steel remains a particularly challenging material to machine, as it is prone to causing substantial tool wear and yielding rough surface finishes (El-Bahloul et al., 2018; Sen et al., 2018).

Corresponding author: Sara A. El-Bahloul – *Production & Mechanical Design Engineering Department, Faculty of Engineering, Mansoura University, Egypt, e-mail:* sara_elbahloul@mans.edu.eg; *Faculty of Engineering, New Mansoura University, Egypt,* sara.elbahloul@nmu.edu.eg

Literature review

Much research has been performed related to stainless steel. Mahmoud Khedr et al. (2023) studied welding of medium-Mn austenitic stainless-steel plates with austenitic NiCr stainless steel and low-carbon steel using gas tungsten arc welding. Mechanical properties were assessed through tensile tests and micro-indentation hardness measurements. Another study by I. Reda Ibrahim et al. (2021) investigated dissimilar butt joints between a low-Ni, medium-Mn austenitic stainless steel and a Ni-Cr austenitic stainless steel using gas tungsten arc welding at varying heat inputs, with ER308 filler metal used. Microstructural analysis and mechanical testing, including tensile strength and hardness properties, were conducted, revealing a duplex structure of austenite matrix and delta ferrite in the fusion zone for joints processed with both low and high energy inputs.

A considerable body of research has been dedicated to the investigation of both EDM and WEDM. Joshi and Pande (2010) provided a finite element based thermo-mechanical model for die-sinking EDM. Their analysis incorporated more plausible assumptions, like the heat flow Gaussian distribution, discharge time and current-based spark radius, and the melting latent heat, to foretell the geometry of crater cavities and MRR. Bialo et al. (2018) presented the machining of metallic composites by EDM in automotive industry.

Relating to WEDM, Boipai (2014) proposed an idea for a model based on finite elements, utilizing ANSYS, to forecast the variation in temperature with respect to pulse on times, as well as the distributed stress in the wire. Patel and Power (2018) employed ANSYS software to examine into the AISI 1040 steel's variation in temperature, considering a heat source with Gaussian distribution. Their analytical model accounted for multi-spark phenomena and various process factors. Zhang et al. (2019) employed ANSYS to estimate MRR and surface temperature distribution of a composite tool. The shape of the discharge crater was determined using the element birth and death method. Shahane and Pande (2016) introduced a novel approach utilizing ANSYS to compute MRR in WEDM. Their results were validated against experimental and numerical findings.

According to different WEDM optimization techniques, Okada et al. (2015) studied the phenomenon of wire breakage and deflection induced by the forceful impingement of the high-pressure nozzle jet during the flushing process. Ho et al. (2016) observed the residual strain quantification in aluminum through the utilization of digital image correlation techniques.

Sivaram et al. (2017) utilized Taguchi methodology for the systematic refinement of machining parameters to achieve enhanced process efficiency. Ebisu et al. (2018) studied on jet flushing's effects on the geometric precision of corner profiles. El-Bahloul (2020) optimized the WEDM process of AISI304 stainless steel using statistical approaches in conjunction with artificial intelligence methodologies. The outcomes revealed that although a reduced MRR was achieved, surface roughness could be optimized by raising the pulse off time while reducing the pulse on time and current. El-mahalawy et al. (2021) conducted experimental optimization of machining factors, including pulse on time, current, voltage, pulse off time, and wire speed, using the Taguchi L32 orthogonal array to evaluate the resulting MRR and surface abrasion. El-Bahloul and Mostafa (2021) presented a statistical and experimental Optimization for hipped Udimet700 while machining by WEDM. The optimal condition that correlated to a greater MRR and microhardness while obtaining a lower surface roughness was discovered via the proposed coupled approach.

Consequently, a multitude of scholars are diligently engaged in the pursuit of empirically quantifying MRR and fine-tuning the various machining parameters, whereas the scope of numerical investigations remains comparatively limited. The primary purpose of this investigation is to develop a comprehensive thermo-structural model for WEDM, specifically tailored for the calculation of MRR during the machining process of AISI304 stainless steel. Subsequently, experimental observations were employed to validate the anticipated outcomes derived from the computational model constructed using ABAQUS software.

Materials & Methods

Thermo-Mechanical Finite Element Modeling of WEDM

The working principle underlying WEDM involves the reduction of the distance between the two electrodes, namely the workpiece and the wire. This reduction causes an increase in the electric field strength within the gap, surpassing the dielectric's strength. Consequently, the dielectric breaks, enabling the flow of current between the two electrodes, thereby giving rise to the generation of sparks. To mathematically describe the temperature variation along both the workpiece and the wire, the following assumptions are (Boipai, 2014; Kumar, 2014):

- The model is specifically designed for an only one spark event.

- The on time for the pulse and the discharge duration are assumed to be identical for each individual pulse.
- The analysis focuses on an axisymmetric work domain.
- The particular type of wire is presumed to be uniform, isotropic, and characterized by stable properties.
- Variations in temperature and vibration impacts that span the wire's diameter are neglected.
- The workpiece is assumed to have an isotropic and homogeneous material composition.
- The workpiece's compositional characteristics are considered in the context of temperature and are free from any pre-existing stress prior to the machining process.
- The workpiece material thermal expansion does not affect the shape and density of the individual elements.
- The heat flux distribution on the workpiece's surface is anticipated to follow a Gaussian distribution.
- The temperature analysis is regarded as a transient type of analysis.
- Although the diameter of the heat source or discharge channel depends on the discharge duration, a continual worth matching to the end of the discharge is utilized throughout the entire time period.

This research endeavor aims to devise coupled temperature displacement ABAQUS models tailored to the specifications of AISI304 Stainless Steel. To facilitate these simulations, Visual Studio and Intel Parallel Studio have been configured to seamlessly interface with ABAQUS, bolstering its computational capabilities by code development. Subsequently, the essential parameters, namely motion, voltage, current, and heat flux, have been meticulously defined in a subroutine and subsequently imported into ABAQUS.

Modeled Workpiece and Tool

Significant quantities of thermal energy are generated during the WEDM procedure, necessitating the evaluation of material characteristics relevant to this process. The AISI 304 stainless steel Johnson–Cook parameters and the material's mechanical characteristics are presented in Table 1. Additionally, Table 2 provides a comprehensive overview of the properties pertaining to the molybdenum wire. For the purpose of this investigation, a criteria for the onset of ductile damage, along with a fracture strain value of 1.5, has been adopted.

Utilizing the ABAQUS/EXPLICIT software, a three-dimensional representation of both the workpiece and the tool was constructed. The workpiece was modeled as a cuboid having a thickness of 5 mm and a cross-sectional area of 10×10 mm^2. On the

other hand, the wire was represented as a solid cylinder with 0.18 mm diameter. The workpiece and the tool were discretized using the C3D8RT element type, as illustrated in Fig. 2. For the tool path, the mesh of the workpiece was refined to account for the deformation that occurs during the cutting process. Due to excessive distortion of certain elements in the thermoplastic cutting simulation, an element deletion approach was implemented.
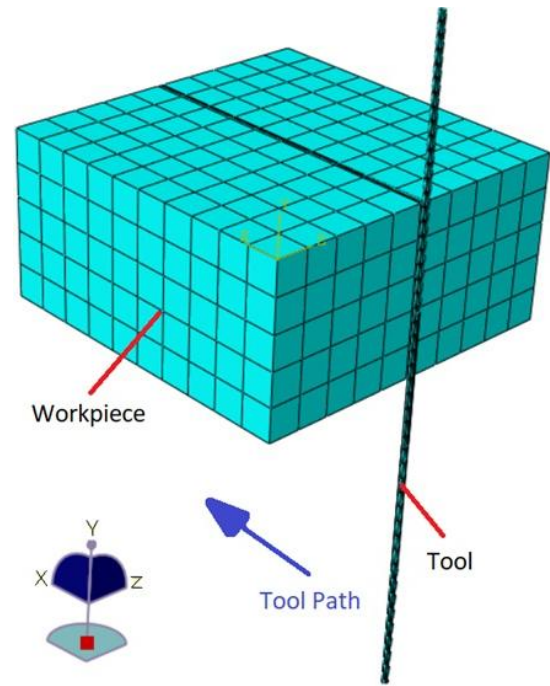
Fig. 2. The workpiece's and tool's undeformed model meshing

Table 1
Mechanical and thermal properties of AISI 304 stainless steel workpiece

Properties	Value
Thermal Conductivity (W/m.K)	16.2
Density (kg/m^3)	7900
Young's modulus (GPa)	200
Poisson's ratio	0.3
Melting point (°C)	1400
Transition temperature (°C)	727
Specific heat (J/kg.K)	440
Johnson–Cook parameters	A = 310 MPa, B = 1000 MPa, $c = 0.07$, $n = 0.65$, $\dot{\varepsilon_0} = 1 \, \text{s}^{-1}$, and $m = 1$

Table 2
Molybdenum wire properties

Properties	Value
Thermal Conductivity (W/m.K)	139
Linear thermal expansion coefficient (K^{-1})	4.8×10^{-6}
Density (kg/m^3)	10280
Young's modulus (GPa)	329
Poisson's ratio	0.31
Shear modulus (GPa)	126
Melting point (°C)	2523
Specific heat (J/kg.K)	250

Governing Equation, Loads, and Boundary Condition

Within the context of WEDM, the incident of discharge can be characterized as the workpiece undergoing heating due to the interaction with the plasma channel generated by the electrical discharge. In order to scrutinize this process, a specific cylindrical region surrounding the spark location on the workpiece is elected for detailed examination. The axisymmetric form of the workpiece's differential equation for heat diffusion is expressed by Equation (1), which serves as a fundamental tool to assess the nonlinear, transient analysis of the distribution of heat across the workpiece. Conversely, Equation (2) is recognized as the governing equation applicable to the wire utilized.

$$\rho C_p \left[\frac{\partial T}{\partial t} \right] = \left[\frac{1}{r} \frac{\partial}{\partial r} \left(K_r \frac{\partial T}{\partial r} \right) + \frac{\partial}{\partial z} \left(K_r \frac{\partial T}{\partial z} \right) \right] \quad (1)$$

where ρ is the density, C_p is the specific heat, K_r is the workpiece thermal conductivity, t is the time, and T is the temperature.

$$\rho C \left[\frac{\partial T}{\partial t} \right] = \left[\frac{\partial}{\partial r} \left(K_w \frac{\partial T}{\partial r} \right) \right.$$
$$\left. + \frac{1}{r^2} \frac{\partial}{\partial \theta} \left(K_w \frac{\partial T}{\partial z} \right) + \frac{\partial}{\partial z} \left(K_w \frac{\partial T}{\partial z} \right) + q'' \right] \quad (2)$$

where z is the axial coordinate, θ and r are the angle and radial coordinates respectively, C and ρ are the wire material specific heat and the density, K_w is the wire material thermal conductivity, and T is temperature of the wire's micro element.

The depicted region in Fig. 3 represents the specific area of interest for analysis in this study. The workpiece exhibits axisymmetric properties with respect to the z-axis, and a particular region denoted as R has been extracted from the workpiece. Employing a Gaussian distribution, a heat flux corresponding to an only one spark is utilized. solely on surface 1, up

to the boundary defined by region R. The influence of convection heat transfer, resulting from the cooling effect of the dielectric fluid, is considered on the remainder of surface 1. Surfaces 4 and 3, located at a considerable distance from the spark radius, do not participate in the heat transmission process as the spark only makes momentary contact. The heat flux value for the axisymmetric surface 2 is intentionally set to zero. Consequently, the circumstances at the boundaries for the various surfaces of the workpiece are established in accordance with Equations (3), (4), and (5). Equation (3) pertains to the boundary up to the spark radius R, Equation (4) is applicable beyond the spark radius R, and Equation (5) encompasses the boundary conditions for surfaces 2, 3, and 4 (Maradia and Wegener, 2015).

$$K_r \frac{\partial T}{\partial z} = Q(r) \quad (3)$$

$$K_r \frac{\partial T}{\partial z} = h_c(T - T_o) \quad (4)$$

$$\frac{\partial T}{\partial z} = 0 \quad (5)$$

where h_c is the rate of heat transfer between the dielectric and the workpiece surface, $Q(r)$ is the heat flux, and T_o is the room temperature.

The boundary conditions for the tool surface are set as in Equation (6).

$$K_w \frac{\partial T}{\partial r} = h(T - T_o) \quad (6)$$

where h is the coefficient of the heat transfer, T_o is the initial wire electrode temperature.
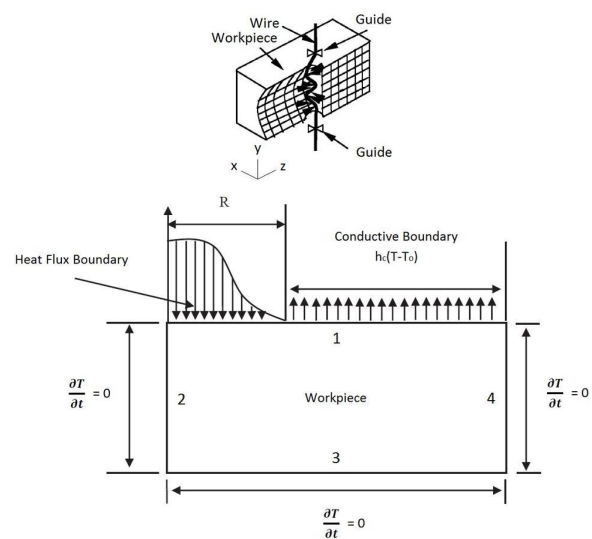
Fig. 3. The WEDM axisymmetric model

In a single spark, the workpiece generates heat that can be calculated by using Equation (7) (Pradhan, 2010). On the other hand, Equation (8) is used to calculate the single spark's wire electrode heat flux (Zhang et al., 2019; Joshi and Pande, 2010).

$$Q\left(r\right) = \frac{4.45 H_i V I}{\pi R^2} e^{-4.5\left(\frac{r}{R}\right)^2} \tag{7}$$

$$Q\left(r\right) = \frac{K_w}{\pi R^2(t)} P V I e^{-\frac{K_w r^2}{R^2(t)}} \tag{8}$$

where $Q(r)$ is the heat flux at the distance from the arc plasma's center r, K_w is the coefficient of heightened heat, R is the arc plasma radius at time t, P is the coefficient of energy distribution, V is the voltage between electrodes, I is the peak current, H_i is heat input on workpiece. The applied heat flux, voltage, and current are equal to 400 W/m^2, 30V, 5A respectively.

In practical application, the extent of spark radius is contingent upon the properties of the surrounding dielectrics, the polarity involved, as well as the materials constituting the electrodes. The precise measurement of spark radius presents a significant challenge due to its exceedingly brief pulse duration, typically on the order of microseconds. Nevertheless, one may employ Equation (9) to calculate the spark radius, as it accounts for discharge power and its temporal characteristics.

$$R\left(t\right) = K I^m t^n \tag{9}$$

where the exponents m, n, and K are empirical constants. These constants' meanings are based on the experimental coefficients N, M, and L are as described in Equation (10) (Datta and Mahapatra, 2010).

$$K = \left(\frac{L}{lm + 0.5N}\right), \ m = M + 0.5N, \ n = N \tag{10}$$

The spark radius in micrometer considering the cutting electrode can be estimated using Equation (11).

$$R = \left(2.04 e^{-3}\right) I^{0.43} t_{on}^{0.44} \tag{11}$$

In accordance with the prescribed model boundary conditions, the workpiece external surface is constrained in all spatial directions, with the exception of the tool path surface, while the wire and workpiece are assumed to be in contact on a surface-to-surface basis. To ensure accurate simulation results, a rigid body constraint is imposed on the tool, thereby preventing any undesired deformation. The tool feed motion is prescribed at a constant rate of 50 mm/min. The emissivity coefficient of AISI304 stainless steel is determined to be 0.54. Utilizing the ABAQUS code, we adopt an assumption of symmetry and Encastre boundary conditions, while imposing a uniform distribution with velocity of $V_1 = 0.06$ mm/s.

Thermal Modeling of MRR

The MRR is influenced by a multitude of factors, including delayed ignition, an abundance of sparks, flush effectiveness, dielectric medium, change in electrodes phase, and erratic behavior of debris. In this study, a comprehensive analysis was conducted to generate a typical crater cavity. The calculation was performed considering a single spark, where the cavity volume was split into various sized cylinders., as illustrated in Fig. 4. To determine the crater volume, it was created a two-dimensional model of the node border. The calculation of the size of a crater left by a single spark was accomplished using Equations (12) and (13) (Priyan et al., 2016).

$$C_{\text{vol}} = \sum_{n=0}^{n-1} V_c \tag{12}$$

$$V_C = \pi \left(\frac{x_n + x_{n+1}}{2}\right)^2 (y_{n+1} - y_n) \tag{13}$$

$$\text{MRR} = \frac{60 \cdot C_{\text{vol}}}{\text{Ton} + \text{Toff}} \tag{14}$$

where C_{vol} is the volume of material removed each discharge pulse, V_c is the disc volume, n is the nodes number, and the coordinates of nodes are x and y.
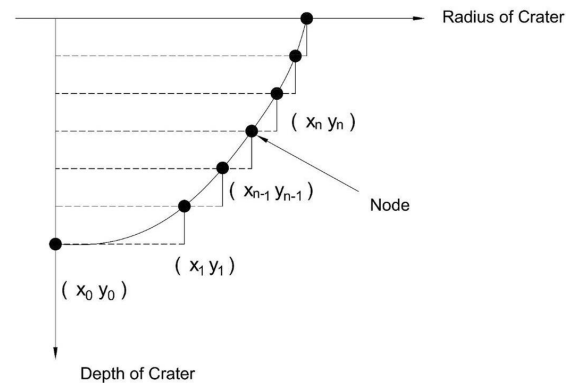
Fig. 4. Estimation modeling of the crater volume

Results

Derived from the antecedent experimental investigations, the machining parameters deemed conducive to attaining the optimal MRR during the process of machining AISI304 stainless steel encompass

a Ton = 45 μs, Toff = 5 μs, and $I = 6$ A. Accordingly, the simulation was performed according to the previous experimental inputs and results (El-Bahloul and Elkhateeb, 2023).

The simulation depicted in Fig. 5 was conducted to analyze the thermal behavior. The modeled experiment machining parameters are Within the Ton period, a substantial temperature rise was observed, leading to the melting of the AISI304 stainless steel material. Subsequently, during the Toff phase, no sparks occurred between the workpiece and the wire, resulting in a cessation of heat flux on the surface of the workpiece. The simulation involved the utilization of a six-node configuration, and the dimensions of these nodes were specified.
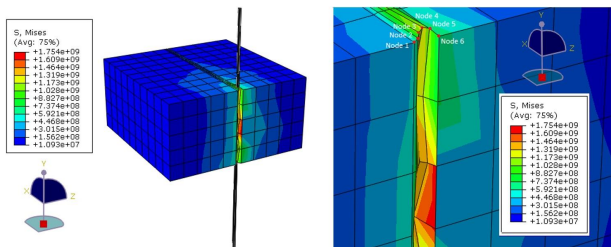
Fig. 5. WEDM simulation utilizing node configuration

The volume of the resultant crater was determined based on the number of nodes employed. Employing Equations (12) to (14), the MRR was computed, and it is equals to 16.638 mm^3/min.

Discussion

The obtained derived numerical MRR value is found to exhibit strong agreement with the MRR value from experimental work. The corresponding MRR values from both the numerical and experimental investigations are presented in Fig. 6 for reference and comparative analysis. The experimental model demonstrates a diminished MRR relative to its numerical counterpart, ascribed to the notable influence of fluid dynamics in attenuating frictional forces.
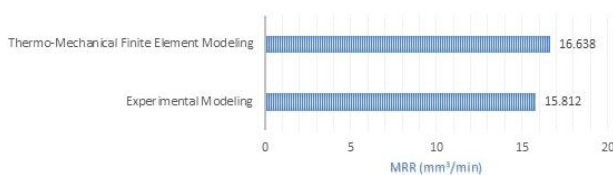
Fig. 6. The resultant MRR based on the experimental and numerical modeling

Conclusions

This research employs the ABAQUS software for Finite Element modeling of WEDM. The obtained results demonstrate a close agreement between the analytically predicted MRR values and the corresponding experimental findings. Specifically, the MRR was measured at 15.812 mm3/min in the experimental work and 16.638 mm^3/min in the numerical simulation. This congruence between the analytical model and experimental study, conducted under identical parameters, attests to the reliability and applicability of the analytical model in further investigations aimed at determining optimal process conditions in WEDM. The achieved MRR value corresponds to the optimal process parameters: $I = 6$ A, Toff = 5 μs, and Ton = 45 μs. Consequently, it is evident that the numerical method employed herein yields reasonably accurate predictions of responses. Hence, this numerical approach offers the potential to forecast outcomes before actual machining operations. Notably, numerical methods are adept at resolving intricate and complex problems beyond the scope of experimental approaches. Additionally, the computational efficiency of numerical methods allows for rapid acquisition of results, making them both time and cost-effective alternatives.

Acknowledgments

References

Bialo D., Peronczyk J., and Skalski A., (2018). Applications of metallic composites in the automotive industry and their machining by the EDM. *Journal of KONES Powertrain and Transport*, 1(1), DOI: 10.5604/01.3001.0012.2440.

Bobbili R., Madhu V., and Gogia A. (2015). Multi response optimization of wire-EDM process parameters of ballistic grade aluminium alloy. *Engineering Science and Technology, an International Journal*, 18(4), 720–726, DOI: 10.1016/j.jestch.2015.05.004.

Boipai B. (2014). *FEM analysis for WEDM process.* Master's degree Thesis, National Institute of Technology, Rourkela – 769008.

Datta S., and Mahapatra S., (2010). Modeling, simulation and parametric optimization of wire EDM process using response surface methodology coupled with grey-Taguchi technique. *International Journal of Engineering, Science and Technology*, 2(5), 162–183, DOI: 10.4314/ijest.v2i5.60144.

Ebisu T., Kawata A., Okamoto Y., Okada A., and Kurihara H., (2018). Influence of Jet Flushing on Corner Shape Accuracy in Wire EDM. *Procedia CIRP*, 68, 104–108, DOI: 10.1016/j.procir.2017.12.031.

El-Bahloul, S.A. (2020). Optimization of wire electrical discharge machining using statistical methods coupled with artificial intelligence techniques and soft computing. *SN Applied Sciences*, 2(1), 1–8, DOI: 10.1007/s42452-019-1849-6.

El-Bahloul, S.A., El-Shourbagy, H.E., El-Bahloul, A.M., and El-Midany, T.T. (2018). Experimental and Thermo-Mechanical Modeling Optimization of Thermal Friction Drilling for AISI 304 Stainless steel. *CIRP Journal of Manufacturing Science and Technology*, 20, 84–92.

El-Bahloul, S.A., and Elkhateeb, M.G. (2023). Wire Deflection Investigation during WEDM of AISI 304 Stainless Steel: An Experimental and Numerical Study. *Mansoura Engineering Journal*, 48(6), DOI: 10.58491/2735-4202.3080.

El-Bahloul, S.A., and Mostafa, R. (2021). Experimental and Statistical Optimization Of Wire- EDM For Hipped (HIP) Udimet700. I*nternational Journal of Mechanical & Mechatronics Engineering IJMME-IJENS*, 21(01).

El-Mahalawy, M.M., Samuel, M., Fouda, N., and El-bahloul, S.A. (2021). Investigating the Effect of Wire Electrical Discharge Machining Factors for Ductile Cast Iron (ASTM A536). *International Journal of Industrial Engineering & Production Research.* 32(2), 1–10, DOI: 10.22068/ijiepr.32.2.1.

Ho, C.C., Chang, Y.J., Hsu, J.C., Kuo, C.L., Kuo, S.K., and Lee, G.H. (2016). Residual strain measurement using wire EDM and DIC in aluminum. *Inventions*, 1(1), DOI: 10.3390/inventions1010004.

Ibrahim, I.R., Khedr, M., Mahmoud, T.S., Abdel-Aleem, H.A., and Hamada, A. (2021). Study on the mechanical performance of dissimilar butt joints between low Ni medium-Mn and Ni-Cr austenitic stainless steels processed by gas tungsten arc welding. *Metals (Basel)*, 11(9), DOI: 10.3390/met11091439.

Joshi, S.N. and Pande, S.S. (2010). Thermo-physical modeling of die-sinking EDM process. Journal of Manufacturing Process, 12(1), 45–56, DOI: 10.1016/j.jmapro.2010.02.001.

Khedr, M., Ibrahim, R., Jaskari, M., Ali, M., Abdel-Aleem, H., Mahmoud, T., and Hamada, A. (2023). Microstructural Evolution and Mechanical Performance of Two Joints of Medium-Mn Stainless Steel with Low- and High-Alloyed Steels. *Materials*, 16(4), DOI: 10.3390/ma16041624.

Kumar, A., Kumar, D., and Maity, K.P. (2014). Numerical Modeling of Wire Electrical Discharge Machining of Super alloy Inconel 718. Procedia Engineering, 97, 1512–1523, DOI: 10.1016/j.proeng.2014.12.435.

Kumar, A., Soota, T., and Kumar, J. (2018). Optimisation of wire-cut EDM process parameter by Grey-based response surface methodology. *Journal of Industrial Engineering International*, 14(4), 821–829, DOI: 10.1007/s40092-018-0264-8.

Maradia, U. and Wegener, K. (2015). *EDM Modelling and Simulation.* Book Chapter: 3, Nova Science Publishers.

Mythili, T., and Thanigaivelan, R. (2020). Optimization of wire EDM process parameters on Al6061/Al2O3 composite and its surface integrity studies. *Bulletin of the Polish Academy of Sciences: Technical Sciences*, 68(6), 1403–1412, DOI: 10.24425/bpasts.2020.135382.

Okada, A., Konishi, T., Okamoto, Y., and Kurihara, H. (2015). *Wire breakage and deflection caused by nozzle jet flushing in wire EDM.* CIRP Annals Manufacturing Technology, 64(1), 233–236, DOI: 10.1016/j.cirp.2015.04.034.

Patel, I., and Powar, P. (2018). Fem Analysis With Experimental Results To Study Effect of Edm Parameters on Mrr of Aisi 1040 Steel. *International Research Journal of Engineering and Technology*, 05(09), 1332–1341.

Pradhan, M.K. (2010). *Modeling and Simulation of Thermal Stress in Electrical Discharge Machining Process.* 4th International Conference on Advances in Mechanical Engineering, S.V.N.I.T, Surat, India, pp. 360–364.

Priyan, M., Swin, W., Anand, V., Kelvin, P., Siva, V., (2016). Investigation of Surface Roughness and MRR on Stainless Steel Machined by Wire EDM. *International Journal of Engineering Research*, 5(03), 66–72, DOI: 10.17577/ijertv5is030114.

Sen, R., Choudhuri, B., Barma, J.D., and Chakraborti, P. (2018). Optimization of wire EDM parameters using teaching learning based algorithm during machining of maraging steel 300. *Materials Today. Proceedings*, 5(2), 7541–7551, DOI: 10.1016/j.matpr.2017.11.426.

Shahane, S., and Pande, S.S. (2016). Development of a Thermo-Physical Model for Multi-spark Wire EDM Process. Procedia Manufacturing, 5, 205–219, DOI: 10.1016/j.promfg.2016.08.019.

Sivaram, A.R., Vinoth, V. Kumar, Umanath, K., Sarathkumar, P., and Rajavel, R. (2017). Optimization of machining parameters in wire cut edm using-taguchi techniques. *Journal of Advanced Research in*

Dynamical and Control Systems, 9(2) Special Issue, 883–897.

Zhang, S., Zhang, W., Wang, P., Liu, Y., Ma, F., Yang, D., and Sha, Z. (2019). Simulation of material removal process in EDM with composite tools. *Advances in Materials Science and Engineering*, DOI: 10.1155/2019/1321780.